Composition-Dependent Formation of Platinum Silver Nanowires

Zhenmeng Peng,[†,§] Hongjun You,[†,‡,§] and Hong Yang[†,*]

[†]Department of Chemical Engineering, University of Rochester, Rochester, New York 14627-0166 and [‡]Sate Key Laboratory for Mechanical Behavior of Materials, Materials Science and Engineering School, Xi'an Jiaotong University, Xi'an, Shannxi 710049, People's Republic of China. [§]These two authors contributed equally to this work.

ABSTRACT The understanding of shape control of colloidal nanoparticles is still rather limited even after well over a decade of intensive research efforts. While surface capping agents can greatly influence the growth habit of nanocrystals in solution, the formation of certain morphology can hardly be understood based on both experimental data and simulations. Without a good understanding of the origins for shape formation, deterministic approaches to the synthesis of nanostructures can be hard to realize. In this paper, we describe the synthesis and formation of PtAg alloy nanowires in the presence of oleylamine and oleic acid through the oriented attachment. Transmission electron microscopy study shows the formation of wormlike nanowires occurs largely at the composition around $Pt_{50}Ag_{50}$. Both Pt and Ag rich alloy nanostructures form sphere-like or faceted nanoparticles under the same reaction conditions. Density functional theory calculation is used to understand the interactions between the functional groups of capping agents and low index planes of PtAg alloys. The structural order of interfaces after collision between primary particles is obtained by molecular dynamic simulation. The results indicate that the formation of alloy nanowires is mostly driven by the interplay between the binding energy of capping agents on alloy surfaces and the diffusion of atoms at the interface upon the collision of primary nanoparticles.

KEYWORDS: morphology · platinum silver · nanowire · oriented attachment · potential energy · adsorption energy · surface diffusion

The colloidal nanocrystals form through nucleation, followed by a growth process in which nutrients are consumed.[1−7] Recently, *in situ* transmission electron microscopy (TEM) studies show that final resulting nanoparticles can be generated from the primary colloidal nanoclusters.[8−10] In some cases, primary particles can grow into nanowires through oriented attachment.[11−16] For semiconducting quantum dots and oxides, dipolar interaction seems to the key driving force for the formation of such nanowires. The oriented attachment however can lead to the formation of low dimensional morphologies in materials with no permanent dipole as well, suggesting factors other than dipolar interaction may also be important.[11,17−20]

Nanostructured platinum alloys are selected for this study, because they are important in a range of industrial applications, from electronics to catalysts and electrocatalysts.[1,21−25] The needs for green technology and sustainable industrial processes put new challenges in the design and synthesis of highly active and selective nanocatalysts,[26,27] which requires better understanding on how to precisely control crystal morphology, as shape and surface composition of nanocrystals are typically governed by the underlying crystal symmetry. For Pt alloy nanowires, PtAg, PtCo, PtCu, and PtFe have been synthesized in both molecular solvents and ionic liquids.[18,28−34] These alloy nanowires have been obtained through the reduction of metal salts and thermal decomposition of metal carbonyls in the presence of capping agents.[30−34] It has also been found that PtAg not only can form alloys at the nanometer-sized scale, but also possess different nanostructures when they are produced in a nonhydrolytic system.[18]

In this paper, we present the formation of $Pt_{53}Ag_{47}$ nanowires in the presence of oleic acid and oleylamine, while Pt- or Ag-rich alloys form faceted or sphere-like nanoparticles. This composition-dependent growth provides us with a model in understanding the key factors that govern the formation of Pt metal alloy nanowires. In this context, density functional theory (DFT) is used to compare the absorption energy between the functional groups of capping agents and low index surfaces of Pt−Ag alloys, while molecular dynamic (MD) simulation is used to examine the collisions between individual particles and surface atomic diffusion. The experimentally

*Address correspondence to hongyang@che.rochester.edu.

Received for review November 23, 2009 and accepted January 27, 2010.

Published online February 5, 2010.
10.1021/nn9016795

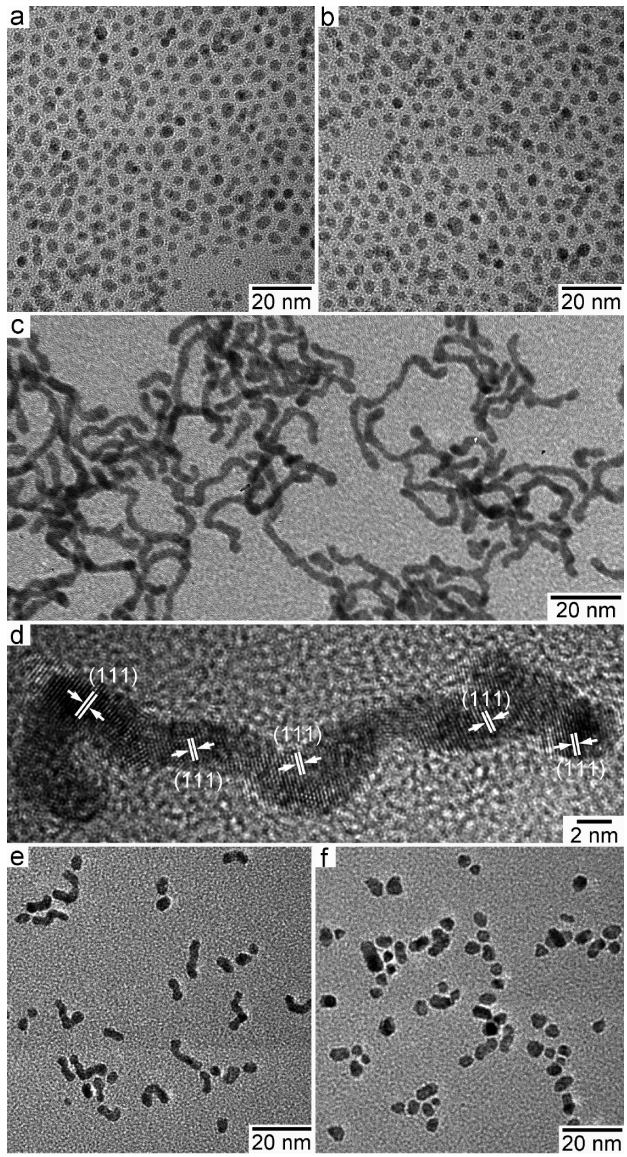

Figure 1. TEM images of (a) $Pt_{26}Ag_{74}$, (b) $Pt_{39}Ag_{61}$, (c, d) $Pt_{53}Ag_{47}$, (e) $Pt_{73}Ag_{27}$, and (f) $Pt_{86}Ag_{14}$ nanostructures, respectively.

observed formation of PtAg nanowire can be explained well by the simulation data.

RESULTS AND DISCUSSION

Experimental Results. Figure 1 shows the TEM images of Pt−Ag nanostructures made at different platinum acetylacetonate/silver stearate ($Pt(acac)_2$/Ag(St)) molar ratios. Energy dispersive X-ray (EDX) analysis was used in obtaining the composition of these alloy nanostructures and the results are summarized in Table 1 (Supporting Information, Figure S1). There was a clear correlation between the shape and composition of Pt−Ag nanostructures. Sphere-like nanoparticles, obtained at $Pt(acac)_2$/Ag(St) molar ratio of 1/4, had an average composition of $Pt_{26}Ag_{74}$ and a diameter of 3.2 ± 0.4 nm (Figure 1a and Table 1). Similarly, 3.4 ± 0.4 nm $Pt_{39}Ag_{61}$ nanoparticles formed at $Pt(acac)_2$/Ag(St) molar ratio of 1/2 (Figure 1b). When this ratio increased to 1/1,

TABLE 1. Compositions of Pt−Ag Alloy Nanostructures Prepared at Different $Pt(acac)_2$/Ag(St) Feeding Ratios

		PtAg nanoalloys[a]		
sample no.	$Pt(acac)_2$/Ag(St) molar ratio	Pt (atom %)	Ag (atom %)	composition
1	1/4	25.6 ± 0.5	74.4 ± 0.5	$Pt_{26}Ag_{74}$
2	1/2	39.2 ± 0.2	60.8 ± 0.2	$Pt_{39}Ag_{61}$
3	1/1	53.1 ± 0.6	46.9 ± 0.6	$Pt_{53}Ag_{47}$
4	2/1	73.1 ± 0.4	26.9 ± 0.4	$Pt_{73}Ag_{27}$
5	4/1	86.4 ± 0.8	13.6 ± 0.8	$Pt_{86}Ag_{14}$

[a]The atomic percentage and composition of the alloys were obtained based on EDX analysis.

the shape of nanoparticles was dominated by wormlike nanowires (Figure 1c). The average diameter of the nanowires was 2.8 ± 0.4 nm based on the TEM measurement. High-resolution TEM (HR-TEM) images reveal that these nanowires were composed of multiple crystalline domains, and the observed fringes were from {111} planes (Figure 1d). The domains of primary crystals were about 3 nm, comparable to diameters of nanoparticles prepared at low $Pt(acac)_2$/Ag(St) molar ratios. These observations suggest the growth of nanowires undergo an oriented attachment process where the primary nanoparticles form first and grow into nanowires.[11,12] EDX analysis indicates that the average composition of these nanowires was $Pt_{53}Ag_{47}$, which was similar to the $Pt(acac)_2$/Ag(St) feeding ratio. The length of the nanowires decreased dramatically when $Pt(acac)_2$/Ag(St) molar ratio was changed to 2/1 (Figure 1e). EDX data indicate that the nanoparticles had an average composition of $Pt_{73}Ag_{27}$. Nanowires could hardly be observed, when $Pt(acac)_2$/Ag(St) molar ratio changed to 4/1, and composition in the resulting nanostructures reached $Pt_{86}Ag_{14}$ (Figure 1f). Supporting Information Figure S2 shows the PXRD pattern of $Pt_{53}Ag_{47}$ nanostructures made at $Pt(acac)_2$/Ag(St) molar ratio of 1/1. The diffraction pattern could be readily indexed to (111), (200), (220), (311), and (222) planes of a face-centered cubic (fcc) lattice and in between those for pure Ag (87-0719, JCPDS-ICDD) and Pt metals (70-2057, JCPDS-ICDD). This observation indicates that Pt and Ag formed alloy in the form of a solid solution.[18] Similar diffraction patterns at different diffraction positions can be obtained for the nanoparticles made at other $Pt(acac)_2$/Ag(St) molar ratios.

The growth of $Pt_{53}Ag_{47}$ nanostructures was further studied by TEM (Figure 2). Both small primary particles and some short rodlike nanostructures formed 2 min after the injection of metal precursors (Figure 2a). With the increase of reaction time, wormlike morphology appeared (Figure 2b,c). The nanowires reached their maximum length after 1 h, and no major changed in morphology even after 3 h (Figure 2d). The width of nanowires changed very little throughout the process, suggesting that these $Pt_{53}Ag_{47}$ nanowires grow from the primary nanoparticles through the oriented attachment.[11,17]

HR-TEM is used to study the shape evolution of $Pt_{53}Ag_{47}$ nanowires and the data show the attachment occurred mostly on {111} facets (Figure 3). Two growth modes, namely, lattice matched attachment (MA) and twinning attachment (TA) were observed. The grain boundary and lattice defect were not obvious if two primary particles attached and grew together *via* the MA mode (Figure 3b). A twin plane with the mirror image-like orientation could be observed if two particles attached through the TA growth on {111} surfaces (Figure 3c). Both linear and bending morphologies could be obtained when additional particles attached to the existing nanostructures through either MA or TA growth (Figure 3d−i).

Theoretical Analysis. The above experimental results indicate that the formation of composition-dependent PtAg nanowires was through the oriented attachment of primary nanoparticles, which is different from those material systems that undergo anisotropic growth. In the later case, the formation of twin planes in the seed crystals is a useful approach to the synthesis of nanowires.[35−37] For instance, the existence of 5-fold twin plane in the seeds is important for reducing the symmetry of Ag nanocrystals, when poly(vinylpyrrolidone) (PVP) is used as the capping agent.[37] These seeds led to the growth of nanowires. For oriented attachment no defect is necessary for the formation of low-dimensional nanostructures.

In a typical wet synthesis, the precursors react to form seeds and subsequently grow into nanoparticles. These nanoparticles are stabilized by capping agents and move in the liquid phase due to Brownian motions. In this colloidal system, the particles collide at a frequency that can be estimated according to the following equation:[38]

$$f = \frac{kT\rho^{2/3}}{3\pi\eta R} \quad (1)$$

where ρ is the density of the nanoparticle with a radius of R in a solution with viscosity of η, and T is temperature. When two nanoparticles get in close proximity with each other, van der Waals forces begin to dominate in the interactions. If surfactant capping agents are present, they most likely adsorb on the various surfaces of nanoparticles to form buffer layers that prevent the nanocrystals from getting in contact with each other. Only under the conditions that nanocrystal surface is loosely protected and the van der Waals interaction is strong enough to overcome the capping effect, the surface atoms can then be in direct contact with each other upon the collision between two particles, and diffuse across the interface to form anisotropic structures. The key factors in determining the formation of nanowires from primary nanoparticles should largely be governed by both the spontaneous exposure of nanocrystal surfaces and the likelihood of bond formation at the interface. The binding strength of capping agents on crystal surfaces can be modeled through calculating the adsorption energy, which is a thermodynamic effect. The effective bond formation, which is a kinetic effect, can be understood based on the surface reconstruction upon the collision between two particles. Such approach has so far not been systematically examined. In this paper, we focus on understanding the effects of these key thermodynamic and kinetic factors on the observed composition-dependent shape evolution of PtAg nanowires.

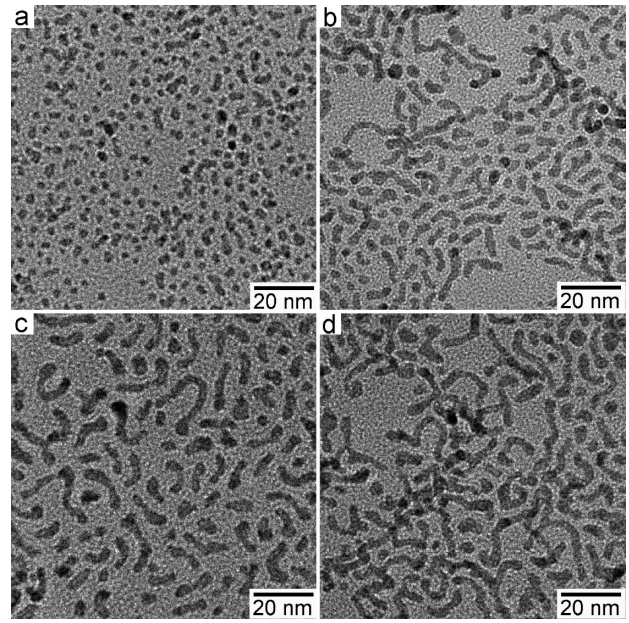

Figure 2. TEM images of $Pt_{53}Ag_{47}$ alloy nanostructures made after the reaction for (a) 2, (b) 10, (c) 30, and (d) 180 min, respectively.

Thermodynamic Effect: Potential Energy of Nanoparticles. The potential energy (E_p) profiles due to atomic interaction between two 3-nm nanoparticles of $Pt_{50}Ag_{50}$ (to mimic composition of $Pt_{53}Ag_{47}$), pure Pt and Ag were calculated using MD simulation (Figure 4, see methods section for details).[39−42] The minimal E_p was obtained when the interparticle distance was around 2.6 Å, roughly equal to the lattice spacing of (111) planes. Further decrease in interparticle distance led to a sharp increase in potential energy, associated with the repulsive forces from the overlapping electrons. The E_p-d profile between two $Pt_{50}Ag_{50}$ nanoparticles resembled those of atomic interactions in some aspects.[43] The values of E_p depended strongly on the composition of nanoparticles, with platinum having the largest decrease in minimal E_p, followed by $Pt_{50}Ag_{50}$. Silver nanoparticles had the smallest decrease in minimal E_p value. This simulation result indicates that if two nanocrystals are in close contact, $Pt_{50}Ag_{50}$ should have more E_p gain than Ag, but less E_p gain than Pt.

Thermodynamic Effect: Adsorption Energy of Functional Groups. As these Pt−Ag nanostructures were produced in solution with capping agents, the effect of oleylamine (OAm) and oleic acid (OA) needs to be considered carefully. In the DFT calculation, carboxylic acid

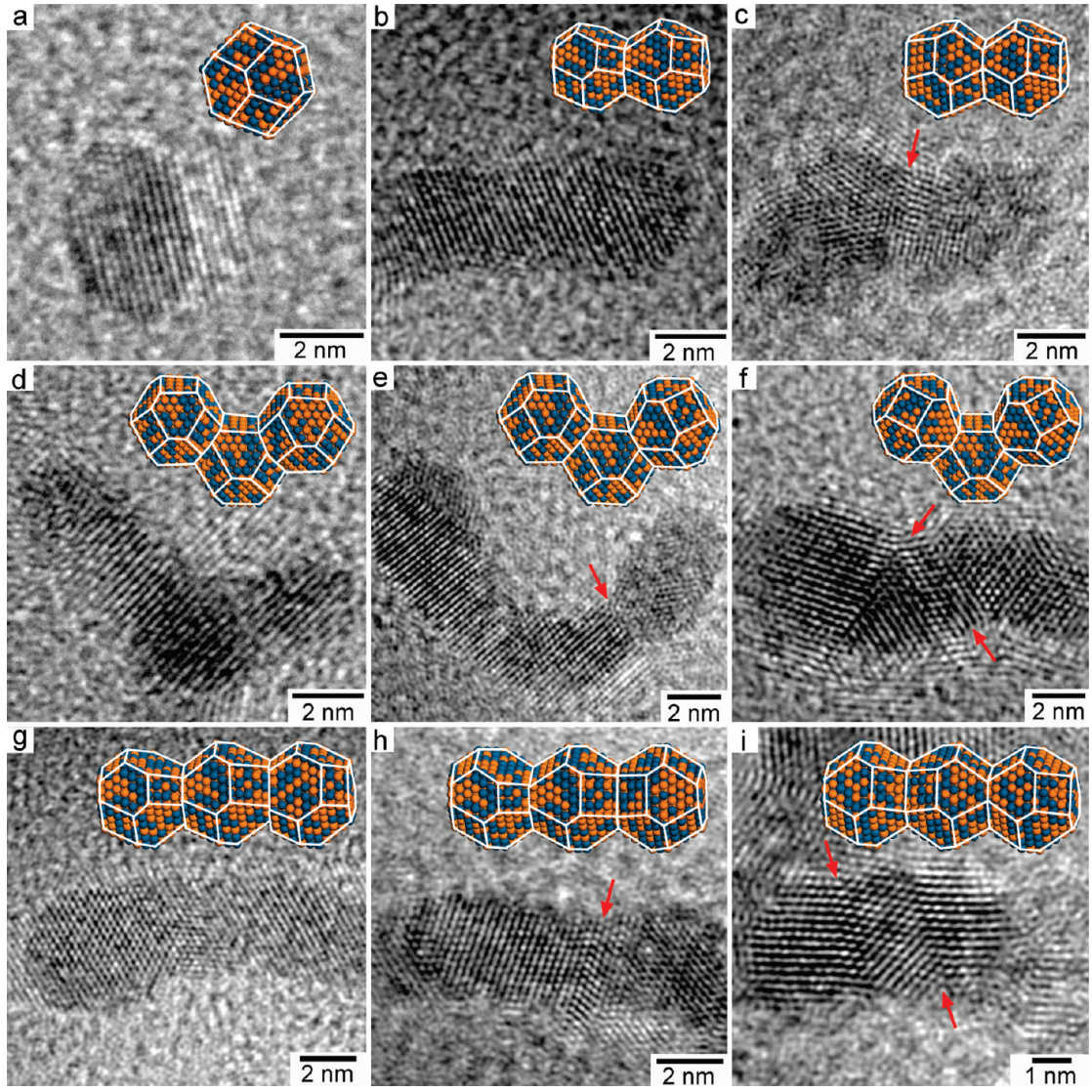

Figure 3. TEM images and the corresponding schematic illustrations showing the early growing stages: (a) a primary particle; two particles connected through (b) MA and (c) TA growths; and (d−i) three particles connected through either MA or TA growth, respectively. The twin planes were indicated by red arrows.

and amine were considered to be the key functional groups in obtaining the adsorption energy (E_{ad}) on metal and metal alloy surfaces. To simplify the simulations, we used short carbon-chain molecules, propylamine and propanoic acid, to model the functional groups of oleylamine and oleic acid, respectively (Supporting Information, Figure S3). This approach was validated by comparing the values of adsorption energy between oleylamine and propylamine on Ag (100) surface. It was found that the E_{ad} was −0.485 eV for oleylamine and −0.491 eV for propylamine. The difference in E_{ad} between these two values was about 1%, which is insignificant. For simplicity, an ordered $Pt_{50}Ag_{50}$ alloy surface was employed in the DFT calculation. For a given family of $Pt_{50}Ag_{50}$ alloy surface, there can be more than one configuration of surface atomic arrangement and for the adsorption of the headgroup of capping agent.

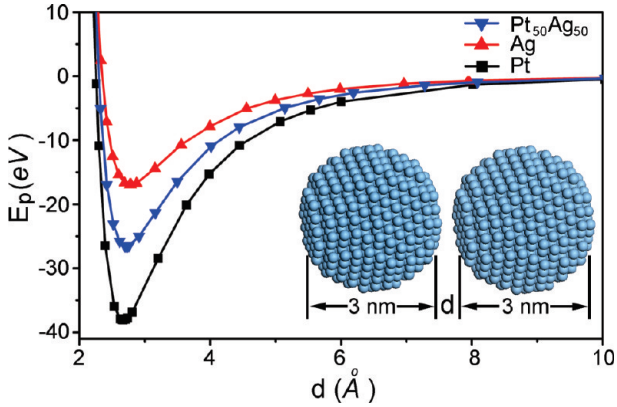

Figure 4. Potential energy (E_p) as a function of distance between two 3-nm $Pt_{50}Ag_{50}$, Pt and Ag nanoparticles.

Figure 5 shows the side and top views of the two most likely configurations of amine functional group on $Pt_{50}Ag_{50}$ {111} surfaces. In this case, the structure of

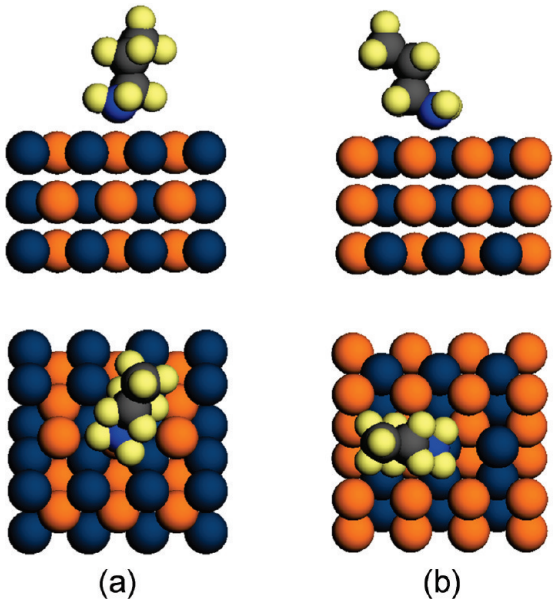

Figure 5. Side (top images) and top (bottom images) views of the two possible configurations of amine functional group on $Pt_{50}Ag_{50}$ {111} surfaces: orange, Ag; dark blue, Pt; yellow, H; gray, C; and blue, N.

adsorbing molecule was fully optimized before the DFT calculation.[44,45] Adsorption energy of the capping agent was obtained by calculating the energy difference before and after the adsorption of functional groups on the $Pt_{50}Ag_{50}$ surfaces. The E_{ad} is −0.762 eV when nitrogen atom is adsorbed on surface Pt atoms, and −0.506 eV when the adsorption is on Ag atoms (Figure 5). The more negative the E_{ad} value is, the stronger the adsorption is. Thus, the more negative E_{ad} value of the two was used to represent the adsorption strength of the functional group on a given surface, when multiple possible configurations for the adsorption on the alloy surface existed. Similarly, there are two possible adsorption configurations of functional group for oleylamine adsorbed on $Pt_{50}Ag_{50}$ {100} surfaces (Supporting Information, Figure S4), and two on $Pt_{50}Ag_{50}$ {110} surfaces (Figure S5), respectively.

For the adsorption of OA on $Pt_{50}Ag_{50}$ surfaces, there should be multiple configurations for the adsorptions on the above three low index $Pt_{50}Ag_{50}$ surfaces because both oxygen atoms of carboxylic acid group can interact with either Pt or Ag atom. Figure 6 shows the four possible adsorption configurations for calculating E_{ad} of OA functional group on $Pt_{50}Ag_{50}$ {111} surfaces using propanoic acid as the model molecule. The calculated adsorption energy ranged from −0.020 eV for the case where carbonyl oxygen of the COOH group adsorbed on Ag atom and the hydroxyl oxygen on Pt atom to −0.139 eV for both oxygen atoms on Ag (Figure 6). There are six most likely configurations for carboxylic group adsorbed on $Pt_{50}Ag_{50}$ {100} surfaces (Supporting Information, Figure S6) and four on $Pt_{50}Ag_{50}$ {110} surfaces (Figure S7). The E_{ad} values were calculated for all these configurations of $Pt_{50}Ag_{50}$ low index surfaces, together with those of pure Pt and Ag metal surfaces. The most negative E_{ad} values represent the strongest adsorptions of amine and carboxyl acid groups on these surfaces and are summarized in Supporting Information, Table S1. These values can be used to compare to the strength of molecular adsorption on surfaces and the ability to prevent the alloy surfaces of primary particles from directly contacting with each other because of the steric hindrance effect of the capping agents.[13,46]

Figure 7 shows bar diagram of these calculated E_{ad} of functional groups for OAm and OA on the three low index surfaces of $Pt_{50}Ag_{50}$ alloys. In general, amine functional group bounded more strongly than carboxylic acid group. Among the configurations of amine func-

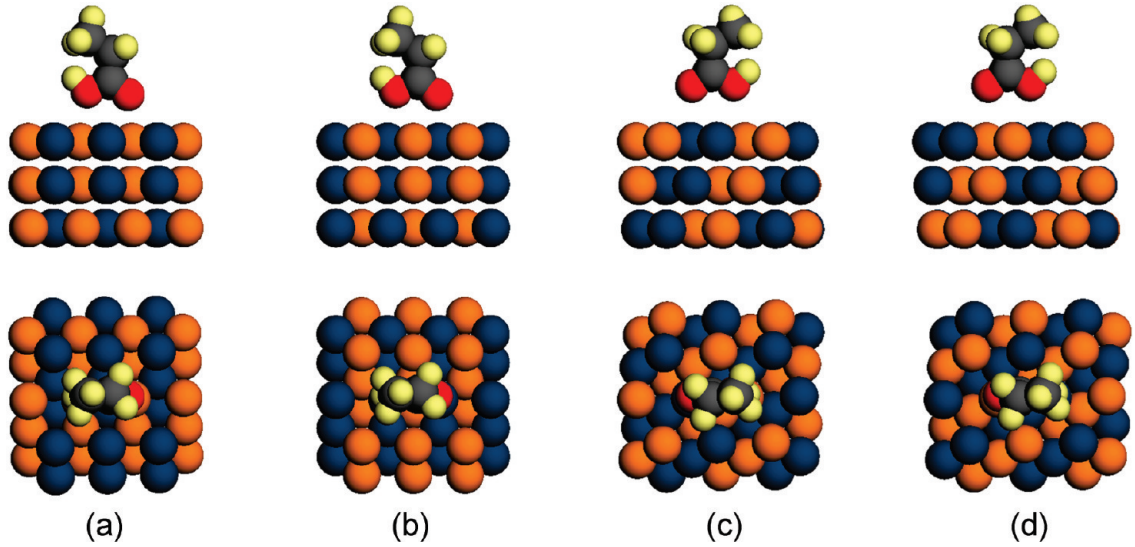

Figure 6. Schematic illustrations of side (top images) and top (bottom images) views of the four possible configurations of carboxylic acid functional group on $Pt_{50}Ag_{50}$ {111} surfaces. The calculated E_{ad} values are (a) −0.139, (b) −0.059, (c) −0.056, and (d) −0.020 eV, respectively: orange, Ag; dark blue, Pt; yellow, H; gray, C; and red, O.

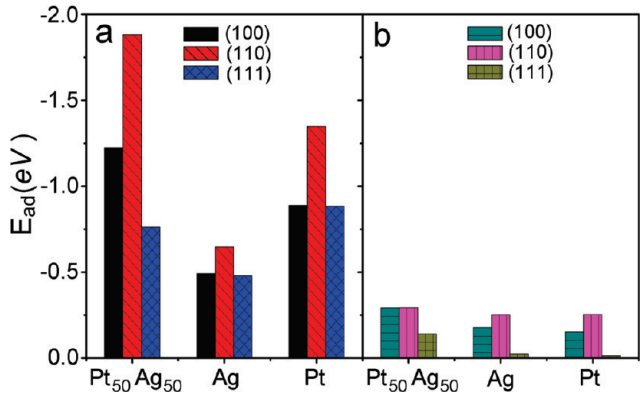

Figure 7. Adsorption energy (E_{ad}) of functional groups for (a) OAm and (b) OA molecules on the three low index surfaces of $Pt_{50}Ag_{50}$, Ag, and Pt, respectively.

tional group on the three low index surfaces, (111) plane had the least negative E_{ad}, suggesting OAm should preferably reside on the surface of nanoparticles and the {111} facets be the least protected by the capping agent. These calculations explain the experimental observation that the oriented growth happened preferably on the {111} surfaces. As the adsorptions of both oleic acid and oleylamine had relatively less negative E_{ad} values on Ag surfaces than those on either $Pt_{50}Ag_{50}$ or Pt, these ligands should displace most readily from Ag nanoparticles, leaving behind the less covered surfaces. However, Ag had the smallest potential energy gain upon collision, which is not favored for the attachment to occur (Figure 4). Experimentally, we observed that Ag nanoparticles could not form wormlike structures under the similar reaction conditions (Figure 8a), suggesting the low potential energy gain should be the main reason for the formation of nanoparticles.

Kinetic Effect: Surface Reconstruction at the Collision Interface. Collision between two primary nanoparticles is only the precondition for the formation of nanowires through oriented attachment. The metal atoms at the colliding interfaces need to form strong metallic bonds in order to grow into nanowires. To understand the bond formation and interfacial structures upon the collision between two nanoparticles, we used MD simulation to obtain the mean square displacements (MSD) as a function of temperature for $Pt_{50}Ag_{50}$ alloy, and Pt and Ag metals (Figure 9a). The results show that Ag atoms could diffuse easily at $Pt_{50}Ag_{50}$ interfacial regions under the reaction temperature of 200 °C (or 473 K). Interestingly, Pt nanoparticles show almost no change in MSD at this temperature. Experimentally, we observed the formation of highly faceted Pt nanoparticles under the same reaction conditions as those for making the wormlike alloy nanowires (Figure 8b) despite the attachment between two Pt nanoparticles is favored thermodynamically based on the analysis of potential energy (Figure 4). The lack of atomic diffusion upon collision suggests that Pt−Pt bond cannot be readily broken and reconstruct at the reaction temperature. Therefore the formation of faceted Pt nanocrystals should largely be determined by this kinetic effect. While Pt atoms in $Pt_{50}Ag_{50}$ alloy had a larger change in MSD value than Pt at 200 °C, Ag atoms in $Pt_{50}Ag_{50}$ alloys had a even more dramatic increase in MSD value than Pt, suggesting the diffusion should be driven preferably by Ag atoms (Figure 9a).

Changes in both particle−particle center distance (D) and total energy (E) of the colliding $Pt_{50}Ag_{50}$ alloy particles were calculated as a function of simulation time (Figure 9b,c). The results indicate that collision between two $Pt_{50}Ag_{50}$ nanoparticles was inelastic as the changes in both D and E were gradual. The particle−particle center distance decreased rapidly after the collision, and the process was dominated by the plastic deformation (Figure 9b). In this inelastic deformation, the nanostructure could go through a reconstruction due to the slide of atomic planes and surface atom diffusion. The primary particles could rotate to match the crystal planes. Our simulation data further indicate that the surface atoms of Pt−Ag alloy particles reorganized and moved fairly rapidly to the neck region between the colliding particles (Supporting Information, Movie S1). This fast movement was likely driven by the difference in chemical potential between the convex and concave regions.[38,47]

The time-dependent pair correlation function ($g(r)$) versus the distance between neighboring atoms to a given atom, r, is used to evaluate the structure order of the interfaces after two $Pt_{50}Ag_{50}$ particles collided (Figure 9d−f). The narrower the peak is, the higher the crystalline order is. The peaks for $Pt_{50}Ag_{50}$ interface became narrow with the increase of simulation time, indicating the atoms in this region changed from disordered to ordered structures. In comparison, two colliding Pt nanoparticles reached stable states in a much shorter simulation time than $Pt_{50}Ag_{50}$ particles, and with little relaxation in both D and E (Figure 10a,b and Supporting Information, Movie S2). The corresponding $g(r)$ as a function of r for Pt nanoparticles show no large lattice deformations (Figure 10c−e). This result suggests that even if two Pt nanoparticles get in contact with each other, reconstruction and the formation of metallic bonds at the interface most likely cannot occur readily.

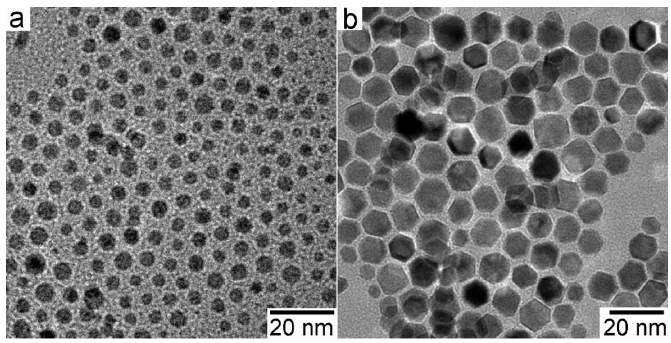

Figure 8. TEM images of (a) Ag and (b) Pt nanoparticles prepared under the same conditions as those for making $Pt_{53}Ag_{47}$ nanowires.

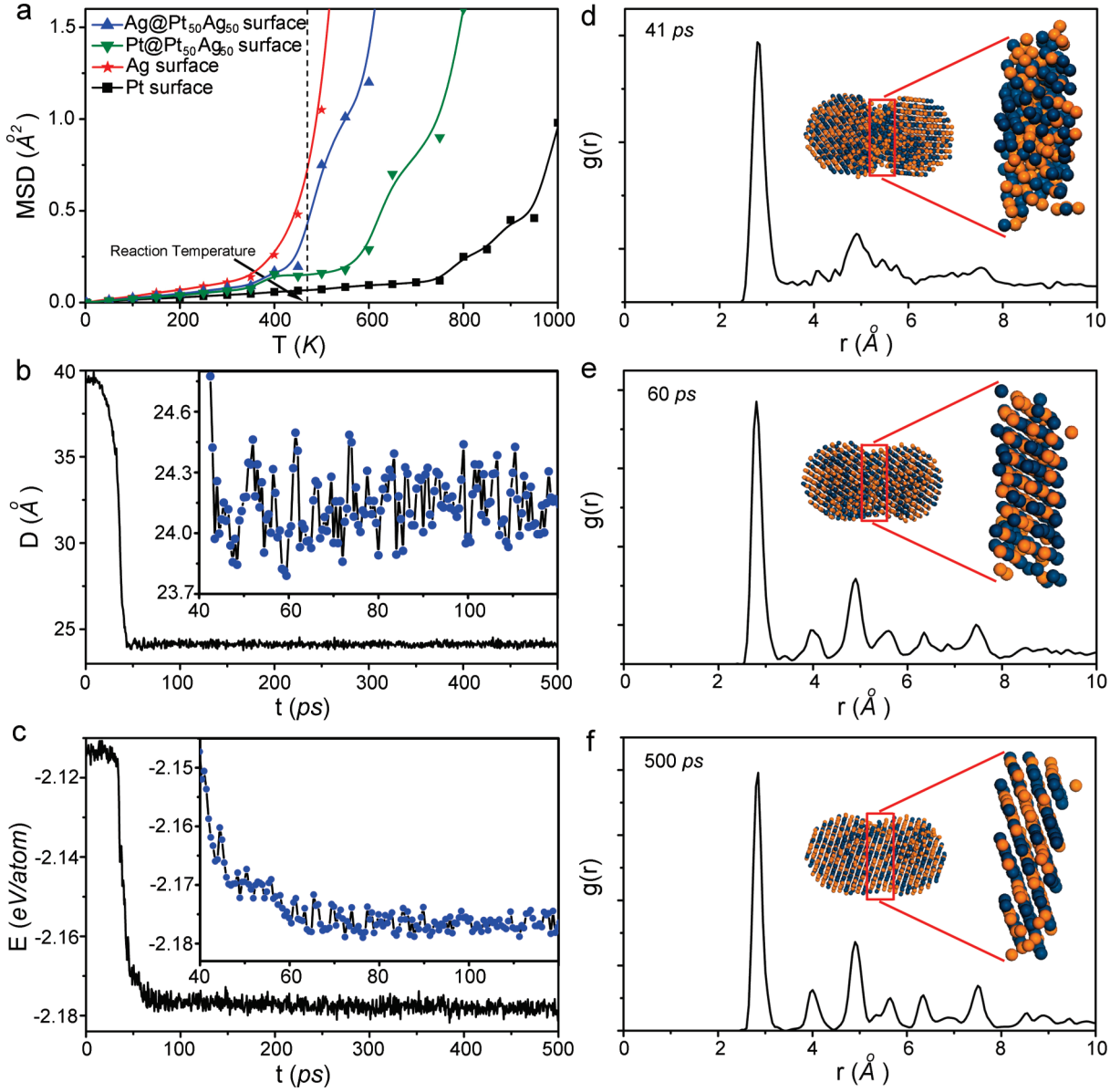

Figure 9. Simulation of time-dependent (a) mean square displacement (MSD) of surface atoms of 3-nm nanoparticles of PtAg alloys, Ag and Pt metals; (b) changes in particle−particle distance (*D*) and (c) total energy (*E*); and (d−f) pair correlation function, g(*r*), as a function of *r* at the interfacial regions between two colliding $Pt_{50}Ag_{50}$ particles.

CONCLUSION

Composition-dependent formation of $Pt_{53}Ag_{47}$ wormlike nanowires provides an excellent platform to understand the key factors for the shape control of Pt alloys. The oriented attachment, which contributes to the formation of metal nanoparticles in a solution, is the dominant mode of formation of Pt−Ag nanowires. Our experimental results, together with the DFT calculation and MD simulation data, indicate that formation of nanowires through oriented attachment is driven by several factors of both thermodynamics (surface adsorption energy and potential energy) and kinetics (surface reconstruction). Thus, a deterministic approach to the shape control of colloidal nanocrystals is plausible by changing the key reaction parameters (such as composition, surface capping agent and reaction temperature) to create synthetic conditions that meet both the thermodynamic and kinetic requirements.

METHODS

Materials. Platinum acetylacetonate ($Pt(acac)_2$, Strem Chemicals, 98%) and silver stearate (Ag(St), Alfa Aesar) were purchased from VWR. Oleic acid (OA, 90%, technical grade), oleylamine (OAm, 70%, technical grade), 1,2-hexadecanediol (HDD, 90%, technical grade), and diphenyl ether (DPE, 99%, ReagentPlus) were purchased from Aldrich. All chemicals and reagents were used as received.

Preparation of PtAg Alloy Nanostructures. All experiments were carried out under argon atmosphere using a standard Schlenk technique. In a typical procedure, HDD (0.49 g or 1.9 mmol), OA (0.3 mL or 0.9 mmol), and OAm (0.3 mL or 0.9 mmol) were mixed with

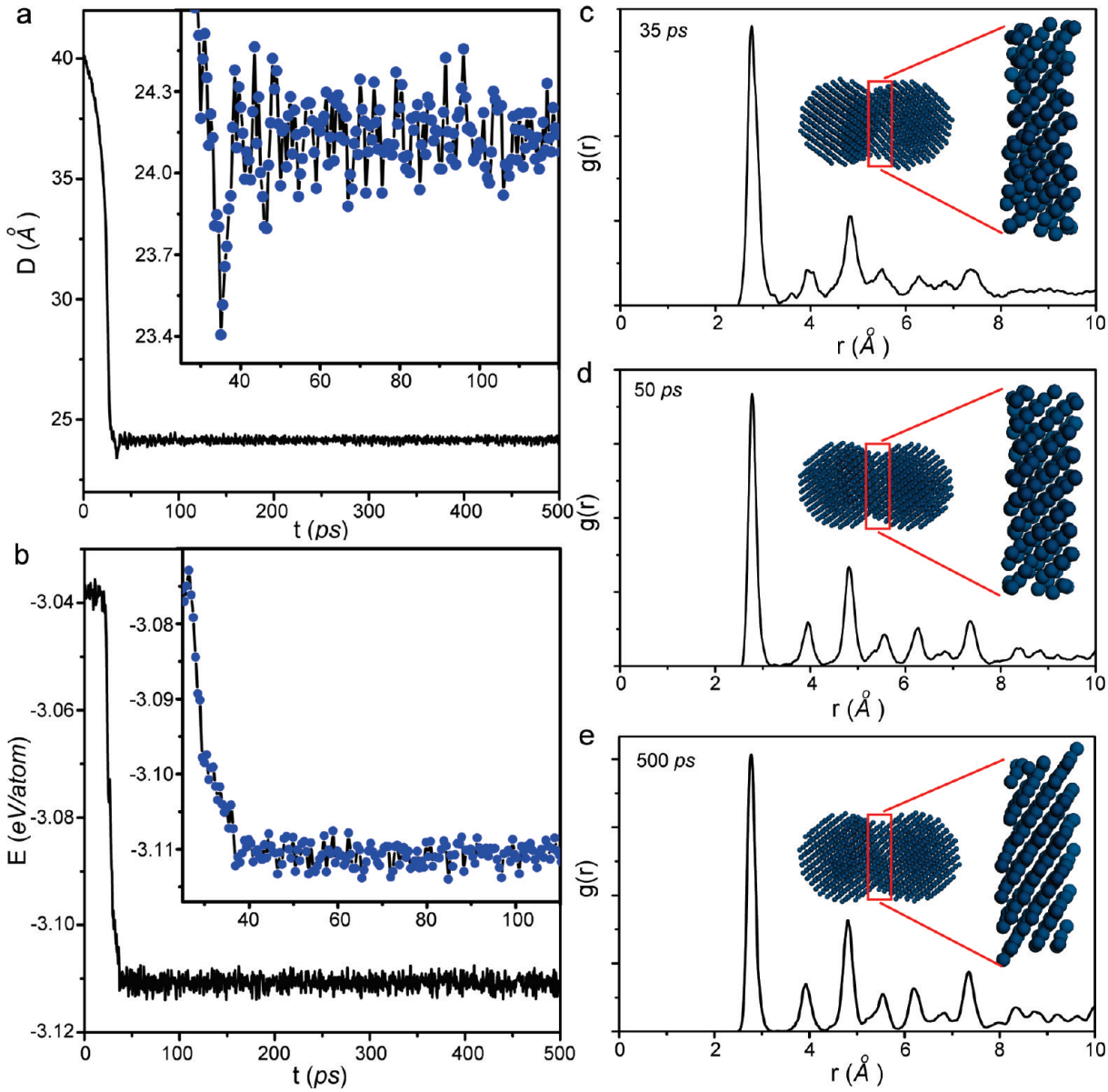

Figure 10. (a) Particle−particle distance (*D*), (b) potential energy (*E*), and (c−e) pair correlation function, g(*r*), as a function of *r* at the interfacial regions of two 3-nm Pt nanoparticles at three different simulation times upon collision.

DPE (4 mL or 25.2 mmol) in a 25-mL three neck round-bottom flask and preheated to 200 °C. In a separate flask, $Pt(acac)_2$ (0.025 g or 0.0625 mmol) and Ag(St) (0.025 g or 0.0625 mmol) were mixed with DPE (1 mL or 6.3 mmol) and heated to 80 °C until all solids were dissolved. The latter solution, which had a light yellow color, was injected into the flask at 200 °C and held for 1 h unless stated otherwise. PtAg alloy nanostructures with different Pt/Ag molar ratios were made by using predetermined amounts of $Pt(acac)_2$ and Ag(St), while keeping the sum of these two precursors constant at 0.125 mmol. For comparison, pure Pt and Ag nanoparticles were prepared using the same procedure. After the reactions, the resulting mixtures were washed twice with 2 mL of hexane and 6 mL of ethanol, followed by centrifugation at 6000 rpm for 5 min. The precipitate was redispersed in 2 mL of hexane for further characterizations.

Characterization. Transmission electron microscopy (TEM) images were taken on a Hitachi 7100 microscope at the accelerating voltage of 80 kV. High-resolution transmission electron microscopy (HR-TEM) images were obtained using a FEI TECNAI F-20 field emission microscope operated at 200 kV, which has an optimal resolution of 1 Å in TEM mode. Energy dispersive X-ray (EDX) analysis on ensembles of nanoparticles was carried out on a field emission scanning electron microscope (FE-SEM, Zeiss-Leo DSM982) installed with an EDAX detector. Powder X-ray diffraction (PXRD) patterns were recorded using a Philips MPD diffractometer with a Cu Kα X-ray source (λ = 1.5405 Å).

DFT Calculation. The Dmol3 code developed by Delley was used to obtain the adsorption energy (E_{ad}) of the two functional groups on metal and alloy surfaces.[44,45] The structures were optimized using Perdew−Wang exchange-correlation function (PW91) based on the generalized gradient approximation (GGA). No symmetry and spin restrictions were applied in the calculation. A double numerical basis set plus a polarization p-function (DNP), DFT semicore pseudopots (DSPP), and an octupole scheme were selected to describe the multipolar expansion of the charge density and Coulomb potential. A thermal smearing of 0.005 hartree (0.136 eV) was set for the energy level of occupied orbits in order for them to converge. The following criteria were used to obtain the optimized final structure. First, convergence tolerance of self-consistent field (SCF) energy was less than 10^{-6} hartree (2.72×10^{-5} eV) in the conjugate gradient algorithm. Second, the maximum displacement of an atom was less than 0.005 Å, and the force due to the displacement was less than 0.002 hartree/Å (0.054 eV/Å). For $Pt_{50}Ag_{50}$ alloy, ordered sur-

faces were used in the simulation. The structures of both capping agents and metal surfaces were fully optimized before they were brought together. The entire structure containing both the adsorbed molecule and metal surface was then optimized to get the most stable form. The E_{ad} was obtained using the following equation:

$$E_{ad} = E_{total} - E_s - E_m \quad (2)$$

where E_{total}, E_s, and E_m are the bond energy of the whole system, metal surface, and free molecule, respectively.

MD Simulation. The MD simulations were performed in an atomic number-volume-temperature (NVT) canonical ensemble and the simulation time step was set to be one femtosecond (*fs*) for all calculations. The atomic interactions were described with the PCFF30 force field in the Forcite package, which is obtained by using the *ab initio* principle and empirical parameters.[39−42] The potential energy (E_p) between metal nanoparticles was calculated by using two 3-nm particles at an initial distance of 3 nm. Randomly mixed $Pt_{50}Ag_{50}$ nanoparticles were optimized using PCFF force field and then used in all the MD simulations. E_p value was obtained by calculating the difference in total energy of the two particles before (E_i) and after (E_f) the interaction, which can be depicted as

$$E_p = E_f - E_i \quad (3)$$

The atom diffusions on the surface of 3-nm metal nanoparticles were simulated at different temperatures ranging from 2 to 1000 K with a step size of 50 K. A simulation time of 200 ps was used at each temperature. The formation of nanowires due to the attachment of primary nanoparticles was modeled using two fully optimized 3-nm nanoparticles. The initial distance between these two particles was set at 1 nm and the temperature was set at 480 K, which was used in the experiments. Changes in particle−particle distance (*D*), total energy (*E*), and pair correlation function ($g(r)$) as a function of simulation time were calculated.

Acknowledgment. This work was supported by U.S. National Science Foundation (Grant No. DMR-0449849). It made use of Shared Facilities at University of Rochester River Campus EM Lab supported in part by DOE. Z.M.P. is a Hooker Fellowship recipient, and H.J.Y. holds a CSC Scholarship.

Supporting Information Available: EDX analysis of Pt−Ag nanostructures (Figure S1), XRD pattern of $Pt_{53}Ag_{47}$ nanowires (Figure S2), models for calculating the adsorption energy of the functional groups on $Pt_{50}Ag_{50}$ surfaces using DFT calculation (Figure S3−S7), and the most negative adsorption energy of the functional groups for oleylamine and oleic acid on low index surfaces of Ag, Pt and $Pt_{50}Ag_{50}$ (Table S1). This material is available free of charge *via* the Internet at http://pubs.acs.org.

REFERENCES AND NOTES

1. Peng, Z. M.; Yang, H. Designer Platinum Nanoparticles: Control of Shape, Composition in Alloy, Nanostructure and Electrocatalytic Property. *Nano Today* **2009**, *4*, 143–164.
2. Xia, Y. N.; Xiong, Y. J.; Lim, B.; Skrabalak, S. E. Shape-Controlled Synthesis of Metal Nanocrystals: Simple Chemistry Meets Complex Physics? *Angew. Chem., Int. Ed.* **2009**, *48*, 60–103.
3. Yin, Y. D.; Alivisatos, A. P. Colloidal Nanocrystal Synthesis and the Organic−Inorganic Interface. *Nature* **2005**, *437*, 664–670.
4. Tao, A. R.; Habas, S.; Yang, P. D. Shape Control of Colloidal Metal Nanocrystals. *Small* **2008**, *4*, 310–325.
5. Park, J.; Joo, J.; Kwon, S. G.; Jang, Y.; Hyeon, T. Synthesis of Monodisperse Spherical Nanocrystals. *Angew. Chem., Int. Ed.* **2007**, *46*, 4630–4660.
6. Sugimoto, T.; Shiba, F.; Sekiguchi, T.; Itoh, H. Spontaneous Nucleation of Monodisperse Silver Halide Particles from Homogeneous Gelatin Solution I: Silver Chloride. *Colloid Surf. A,* **2000**, *164*, 183–203.
7. Mullin, J. W. *Crystallization,* 3rd ed.; Oxford University Press: Oxford, 1997.
8. Zheng, H. M.; Smith, R. K.; Jun, Y. W.; Kisielowski, C.; Dahmen, U.; Alivisatos, A. P. Observation of Single Colloidal Platinum Nanocrystal Growth Trajectories. *Science* **2009**, *324*, 1309–1312.
9. Watzky, M. A.; Finney, E. E.; Finke, R. G. Transition-Metal Nanocluster Size *vs* Formation Time and the Catalytically Effective Nucleus Number: A Mechanism-Based Treatment. *J. Am. Chem. Soc.* **2008**, *130*, 11959–11969.
10. Penn, R. L.; Banfield, J. F. Imperfect oriented Attachment: Dislocation Generation in Defect-Free Nanocrystals. *Science* **1998**, *281*, 969–971.
11. Cademartiri, L.; Ozin, G. A. Ultrathin Nanowires—A Materials Chemistry Perspective. *Adv. Mater.* **2009**, *21*, 1013–1020.
12. Tang, Z. Y.; Kotov, N. A. One-Dimensional Assemblies of Nanoparticles: Preparation, Properties, And Promise. *Adv. Mater.* **2005**, *17*, 951–962.
13. Zhang, Q.; Liu, S. J.; Yu, S. H. Recent Advances in Oriented Attachment Growth and Synthesis of Functional Materials: Concept, Evidence, Mechanism, And Future. *J. Mater. Chem.* **2009**, *19*, 191–207.
14. Pradhan, N.; Xu, H. F.; Peng, X. G. Colloidal CdSe Quantum Wires by Oriented Attachment. *Nano Lett.* **2006**, *6*, 720–724.
15. Banfield, J. F.; Welch, S. A.; Zhang, H. Z.; Ebert, T. T.; Penn, R. L. Aggregation-Based Crystal Growth and Microstructure Development in Natural Iron Oxyhydroxide Biomineralization Products. *Science* **2000**, *289*, 751–754.
16. Cademartiri, L.; Malakooti, R.; O'Brien, P. G.; Migliori, A.; Petrov, S.; Kherani, N. P.; Ozin, G. A. Large-Scale Synthesis of Ultrathin Bi_2S_3 Necklace Nanowires. *Angew. Chem., Int. Ed.* **2008**, *47*, 3814–3817.
17. Teng, X. W.; Han, W. Q.; Ku, W.; Hucker, M. Synthesis of Ultrathin Palladium and Platinum Nanowires and a Study of Their Magnetic Properties. *Angew. Chem. Int. Ed.* **2008**, *47*, 2055–2058.
18. Peng, Z. M.; Yang, H. Ag-Pt Alloy Nanoparticles with the Compositions in the Miscibility Gap. *J. Solid State Chem.* **2008**, *181*, 1546–1551.
19. Fenske, D.; Borchert, H.; Kehres, J.; Kroger, R.; Parisi, J.; Kolny-Olesiak, J. Colloidal Synthesis of Pt Nanoparticles: On the Formation and Stability of Nanowires. *Langmuir* **2008**, *24*, 9011–9016.
20. Fang, J. X.; You, H. J.; Kong, P.; Yi, Y.; Song, X. P.; Ding, B. J. Dendritic Silver Nanostructure Growth and Evolution in Replacement Reaction. *Cryst. Growth Des.* **2007**, *7*, 864–867.
21. Burda, C.; Chen, X. B.; Narayanan, R.; El-Sayed, M. A. Chemistry and Properties of Nanocrystals of Different Shapes. *Chem. Rev.* **2005**, *105*, 1025–1102.
22. Gasteiger, H. A.; Kocha, S. S.; Sompalli, B.; Wagner, F. T. Activity Benchmarks and Requirements for Pt, Pt-Alloy, and Non-Pt Oxygen Reduction Catalysts for PEMFCs. *Appl. Catal. B* **2005**, *56*, 9–35.
23. Burch, R.; Breen, J. P.; Meunier, F. C. A Review of the Selective Reduction Of NOx, with Hydrocarbons under Lean-Burn Conditions with Non-Zeolitic Oxide and Platinum Group Metal Catalysts. *Appl. Catal. B* **2002**, *39*, 283–303.
24. Chen, J. Y.; Lim, B.; Lee, E. P.; Xia, Y. N. Shape-Controlled Synthesis of Platinum Nanocrystals for Catalytic and Electrocatalytic Applications. *Nano Today* **2009**, *4*, 81–95.
25. Sun, S. H. Recent Advances in Chemical Synthesis, Self-Assembly, and Applications of FePt Nanoparticles. *Adv. Mater.* **2006**, *18*, 393–403.
26. Somorjai, G. A.; Rioux, R. M. High Technology Catalysts towards 100% Selectivity Fabrication, Characterization and Reaction Studies. *Catal. Today* **2005**, *100*, 201–215.
27. Lee, E. P.; Peng, Z. M.; Cate, D. M.; Yang, H.; Campbell, C. T.; Xia, Y. Growing Pt Nanowires As a Densely Packed Array on Metal Gauze. *J. Am. Chem. Soc.* **2007**, *129*, 10634–10635.

28. Wang, Y.; Yang, H. Synthesis of CoPt Nanorods in Ionic Liquids. *J. Am. Chem. Soc.* **2005**, *127*, 5316–5317.
29. Zhang, Z. T.; Blom, D. A.; Gai, Z.; Thompson, J. R.; Shen, J.; Dai, S. High-Yield Solvothermal Formation of Magnetic CoPt Alloy Nanowires. *J. Am. Chem. Soc.* **2003**, *125*, 7528–7529.
30. Maksimuk, S.; Yang, S. C.; Peng, Z. M.; Yang, H. Synthesis and Characterization of Ordered Intermetallic PtPb Nanorods. *J. Am. Chem. Soc.* **2007**, *129*, 8684–8685.
31. Yang, S. C.; Peng, Z. M.; Yang, H. Platinum lead Nanostructures: Formation, Phase Behavior, And Electrocatalytic Properties. *Adv. Funct. Mater.* **2008**, *18*, 2745–2753.
32. Chen, M.; Pica, T.; Jiang, Y. B.; Li, P.; Yano, K.; Liu, J. P.; Datye, A. K.; Fan, H. Y. Synthesis and Self-Assembly of fcc Phase FePt Nanorods. *J. Am. Chem. Soc.* **2007**, *129*, 6348–6349.
33. Wang, C.; Hou, Y. L.; Kim, J. M.; Sun, S. H. A General Strategy for Synthesizing FePt Nanowires and Nanorods. *Angew. Chem., Int. Ed.* **2007**, *46*, 6333–6335.
34. Liu, Q. S.; Yan, Z.; Henderson, N. L.; Bauer, J. C.; Goodman, D. W.; Batteas, J. D.; Schaak, R. E. Synthesis of CuPt Nanorod Catalysts with Tunable Lengths. *J. Am. Chem. Soc.* **2009**, *131*, 5720–5721.
35. Maksimuk, S.; Teng, X. W.; Yang, H. Roles of Twin Defects in the Formation of Platinum Multipod Nanocrystals. *J. Phys. Chem. C* **2007**, *111*, 14312–14319.
36. Teng, X. W.; Yang, H. Synthesis of Platinum Multipods: An Induced Anisotropic Growth. *Nano Lett.* **2005**, *5*, 885–891.
37. Wiley, B.; Sun, Y. G.; Mayers, B.; Xia, Y. N. Shape-Controlled Synthesis of Metal Nanostructures: The Case of Silver. *Chem. Eur. J.* **2005**, *11*, 454–463.
38. Halder, A.; Ravishankar, N. Ultrafine Single-Crystalline Gold Nanowire Arrays by Oriented Attachment. *Adv. Mater.* **2007**, *19*, 1854–1858.
39. Sun, H. Force-Field for Computation of Conformational Energies, Structures, And Vibrational Frequencies of Aromatic Polyesters. *J. Comput. Chem.* **1994**, *15*, 752–768.
40. Sun, H.; Mumby, S. J.; Maple, J. R.; Hagler, A. T. An *ab Initio* CFF93 All-Atom Force-Field for Polycarbonates. *J. Am. Chem. Soc.* **1994**, *116*, 2978–2987.
41. Sun, H. Ab-Initio Calculations and Force-Field Development for Computer-Simulation of Polysilanes. *Macromolecules* **1995**, *28*, 701–712.
42. Hill, J. R.; Sauer, J. Molecular Mechanics Potential for Silica and Zeolite Catalysts Based on ab-Initio Calculations. 1. Dense and Microporous Silica. *J. Phys. Chem.* **1994**, *98*, 1238–1244.
43. Kittel, C. *Introduction to Solid State Physics;* Wiley: New York, 1971.
44. Delley, B. An All-Electron Numberical-Method for Solving the Local Density Funciatonal for Polyatomic-Molecules. *J. Chem. Phys.* **1990**, *92*, 508–517.
45. Delley, B. From Molecules to Solids with the DMol(3) Approach. *J. Chem. Phys.* **2000**, *113*, 7756–7764.
46. Bishop, K. J. M.; Wilmer, C. E.; Siowling, S.; Grzybowski, B. A. Nanoscale Forces and Their Uses in Self-Assembly. *Small* **2009**, *5*, 1600–1630.
47. Koparde, V. N.; Cummings, P. T. Molecular Dynamics Simulation of Titanium Dioxide Nanoparticle Sintering. *J. Phys. Chem. B* **2005**, *109*, 24280–24287.